Rare Metal Materials and Engineering
Volume 52, Issue 9, September 2023
Available online at www.rmme.ac.cn

Science Press

Cite this article as: Xu Guangtao, Yang Wei, Liu Hailang, et al. Numerical Simulation and Experiment of Dilution Ratio for Electron Beam Cladding of Inconel 718 Alloy[J]. Rare Metal Materials and Engineering, 2023, 52(09): 3047-3055.

ARTICLE

Numerical Simulation and Experiment of Dilution Ratio for Electron Beam Cladding of Inconel 718 Alloy

Xu Guangtao[1], Yang Wei[1], Liu Hailang[2], Peng Zhiguo[2], Liu Jian[1]

[1] The 30th Research Institute, China Electronics Technology Group Corporation, Chengdu 611730, China; [2] School of Mechanical and Electrical Engineering, Guilin University of Electronic Technology, Guilin 541004, China

Abstract: Based on the distribution law of temperature field in the electron beam cladding process simulated by ANSYS software, the melting depth and melting width of the cross section of cladding layer were investigated, and then the dilution ratio of cladding layer was estimated through simulation. Afterwards, the electron beam cladding experiment was conducted to measure the actual dilution ratio. Through the comparison between simulated and experimental dilution ratios, it can be verified that the dilution ratio of electron beam cladding can be obtained by simulation. The microhardness and the wear resistance of specimen after cladding were investigated. Results show that the smaller the dilution ratio, the better the quality of the cladding layer.

Key words: Inconel 718 alloy; electron beam cladding; temperature field simulation; dilution ratio

Electron beam cladding technique is a forefront surface modification technique[1]. Compared with other processing methods, it has the advantages of high energy density, simple control of process parameters, and free of pollution[2]. In addition, the electron beam cladding can achieve high-precision control of energy distribution and energy input. Thus, the reproducibility of the electron beam cladding is very high. The electron beam cladding can also obtain the cladding layer with excellent forming quality, thereby improving performance of the substrate surface. The quality of electron beam cladding layer is related to the process parameters, but the influence mechanism is still obscure.

Dilution ratio of the preset coating is usually used to evaluate the quality of cladding layer[3]. Mohammed et al[4] studied the influence of process parameters on the dilution ratio of cladding layer during laser cladding. It is found that the dilution ratio is mainly related to the processing power, scanning speed, and wire feeding rate. With increasing the processing power, the dilution ratio of cladding layer is increased. With increasing the scanning speed and wire feeding rate, the dilution ratio of cladding layer is decreased. Zhang et al[5] studied the calculation method to calculate the dilution ratio of laser cladding layers and deduced the quantitative relationship between the dilution ratio of cladding layer and the process parameters. Huang et al[6] studied the calculation method of dilution ratio for laser-induced cladding layer and found that the dilution ratio is related to the induction heating temperature and laser inductive energy. In this research, NiCrBSi coating was prepared by electron beam cladding on Inconel 718 alloy, and the distribution of temperature field in the electron beam cladding was simulated by finite element software. The isotherm diagram of melting point of the substrate and coating materials was analyzed to determine the melting depth and melting width of the cross-section of cladding layer. Then, the dilution ratio was obtained by simulation calculation and experiment. By comparing the simulated and experimental dilution ratios, the accuracy of simulated dilution ratio of cladding layer was verified, providing a novel method to calculate the dilution ratio.

1 Theoretical Analysis

1.1 Simulation theory and results

In the process of electron beam cladding, the specimen surface was scanned by electron beam at a certain scanning rate, resulting in instantaneous temperature change of specimens, namely temperature field[7]. In the three-dimensional thermal

Received date: December 08, 2022
Foundation item: National Major Generic Key Technology Fund Project (2021YFB330104)
Corresponding author: Liu Hailang, Ph. D., Professor, School of Mechanical and Electrical Engineering, Guilin University of Electronic Technology, Guilin 541004, P. R. China, E-mail: 3040944357@qq.com

analysis, the temperature field can be expressed as a function of time t and the coordinates x, y, and z, as follows:

$$\rho c\frac{\partial T}{\partial t}-\frac{\partial}{\partial x}\left(\lambda_x\frac{\partial T}{\partial x}\right)-\frac{\partial}{\partial y}\left(\lambda_y\frac{\partial T}{\partial y}\right)-\frac{\partial}{\partial z}\left(\lambda_z\frac{\partial T}{\partial z}\right)=0 \quad (1)$$

where c is the specific heat capacity of the material (J/kg·°C); ρ denotes the material density (kg/m^3); λ_x, λ_y, and λ_z represent the thermal conductivity of material along x, y, and z directions, respectively (W/m·°C); T is temperature.

The initial temperature during electron beam cladding was room temperature (20 °C), and the boundary conditions only considered the temperature function, heat flux function, and radiative heat flow rate at the specimen boundary[8], as follows:

$$\begin{cases} T_{s_1}=T(x,y,z,t) \\ -\lambda\dfrac{\partial T}{\partial n}=q(x,y,z,t) \\ -\lambda\dfrac{\partial T}{\partial n}=\varepsilon\sigma(T^4-T_a^4) \end{cases} \quad (2)$$

where T_{s_1} is the temperature function of the specimen boundary (°C); λ is the thermal conductivity, which is a constant related to materials (W/m·°C); $\partial T/\partial n$ is the temperature gradient along n direction (° C); q is the heat flow density function (W/m^2); ε is the surface emissivity of specimen, namely blackness; σ is the Stefan-Boltzmann constant of 5.67×10^{-8} W/(m^2·°C^4); T is the temperature on the specimen surface (°C); T_a is the ambient temperature (°C).

The energy of specimen during electron beam cladding was mainly concentrated in the middle part, which conformed to the Gaussian mathematical model. The Gaussian heat source has the advantages of simple model and easy control of process parameters, which can reflect the attenuation law of the electron beam heat source. Therefore, the Gaussian heat source was selected as the heat source model in this research, as indicated by Eq.(3), as follows:

$$q(r)=\frac{3\eta UI}{\pi d^2}\exp\left(-\frac{3r^2}{d^2}\right) \quad (3)$$

where η is the electron beam thermal efficiency (generally η= 0.75); U is the acceleration voltage of the electron beam; I is the beam current of the electron beam; r is the distance from the hot spot to the center of the heat source; d is the effective heating radius of the electron beam.

In the process of electron beam cladding, the coating material and some areas of the substrate undergo the transformation from solid state to liquid state, namely the phase transition. This process involves the absorption and release of latent heat. Latent heat is a non-negligible factor in finite element thermal analysis. However, the phase transition latent heat model is difficult to establish in the simulation. Thus, the latent heat was determined by the enthalpy value[9] in this research. Enthalpy represents the energy transferred by the flow of working medium in the thermal equipment, as expressed by Eq.(4), as follows:

$$\Delta H=\int_{T_0}^{T}\rho c(T)\,\mathrm{d}T \quad (4)$$

where ΔH is enthalpy (J·m^3); ρ is density; c is specific heat; T is the temperature.

For the ANSYS simulation, a reasonable model should be established firstly. In the finite element simulation of electron beam cladding, the solid cuboid model is usually used to simplify the loading of moving heat source[10]. Fig.1 shows the schematic diagrams of simulation model. The size of simulation model was the same as that of the physical model: the length was 50 mm, the width was 30 mm, and the thickness was 11 mm. From the top area to the bottom area of model, there are two parts: the preset coating and the substrate, and their thickness is 1 and 10 mm, respectively. The meshing treatment of the finite element model involves the computational speed, accuracy, and convergence, which is very important in the whole thermal analysis. The coating is directly affected by the electron beam. The heating and cooling rates are extremely high, and the temperature gradient is large. Therefore, in order to accurately reflect the temperature field variation of the coating, the coating was divided into small grids with unit size of 0.5 mm×0.5 mm×0.5 mm, and the substrate was divided into small grids with unit size of 1.0 mm×1.0 mm×1.0 mm.

In the simulation process to determine the pool distribution of the cladding layer, the parameters were set as follows: the electron beam current was 17 mA, the focusing current was 700 mA, and the scanning speed was 10 mm/s. The area with temperature above the melting point of material in the temperature cloud map was regarded as the distribution area of the molten pool of electron beam cladding layer[11]. Thus, the approximate melting range of the cladding layer can be obtained by analyzing the isotherm diagram corresponding to the melting point of the substrate and coating, i. e., the approximate area of the cross-section of the cladding layer.

In the simulation process of laser cladding, the temperature distribution on both sides of the model along the spot center is symmetric, so the temperature distribution on one side of the spot center can sufficiently reflect the temperature distribution on the whole model. Three typical paths were selected: the path on the surface of cladding layer, the path at interface between the coating and substrate, and the path at the center of cladding spot along the molten pool depth, as shown in Fig.2. FH line was located on the surface of cladding layer, which

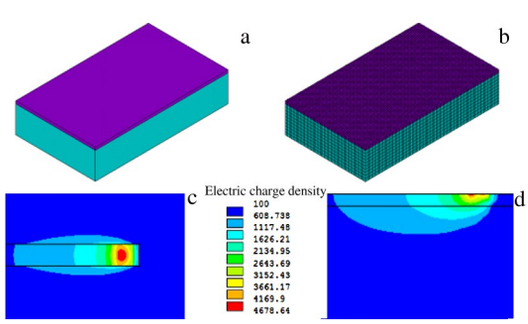

Fig.1 Schematic diagrams of simulation models of electron beam cladding layer before (a) and after (b) meshing; cloud images of surface (c) and cross-section (d) of electron beam cladding layer

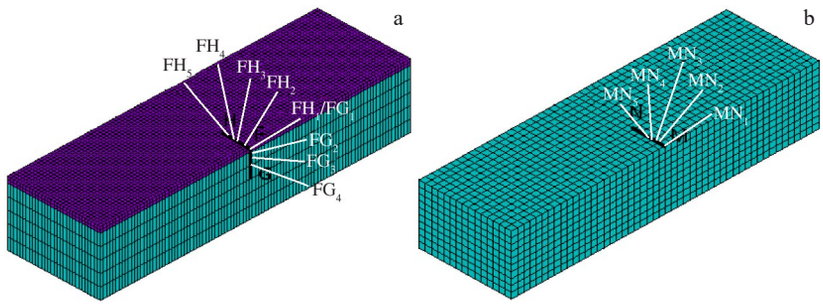

Fig.2 Schematic diagrams of typical paths of cladding layer for simulation: (a) FH and FG lines; (b) MN line

was perpendicular to the movement direction of the cladding spot[12]; FG line was located at the center of the cladding spot along the direction of molten pool depth; MN line was located on the interface between the coating and substrate, which was perpendicular to the movement direction of beam spot. Five points were selected along the FH line on the coating surface, and the segmented lines were named as FH_1=0 mm, FH_2=1 mm, FH_3=2 mm, FH_4=2.5 mm, and FH_5=3 mm. Four points were selected along the FG line along the direction of molten pool depth, and the segmented lines were denoted as FG_1=0 mm, FG_2=0.5 mm, FG_3=1 mm, and FG_4=2 mm. Five points were selected along the MN line at the interface between substrate and coating, and the segmented lines were marked as MN_1=0 mm, MN_2=1 mm, MN_3=1.5 mm, MN_4=2 mm, and MN_5=2.5 mm. According to the longitudinal temperature distribution of specimens, once the longitudinal temperature of the model exceeds the melting temperature of the substrate, the related length is considered as the molten pool depth of substrate. Similarly, at the interface between the substrate and coating, the length of the region with temperature above the melting point of substrate is considered as the width of the molten pool. The length of molten pool of the cladding layer can be determined by the length of the area with temperature above the melting point of coating.

1.2 Simulated cross-section of electron beam cladding layer

Fig.3 shows the temperature distribution of selected points on different typical paths. Fig. 4 shows the variation of maximum temperature of the electron beam cladding layer at different distances away from the beam spot center on different typical paths. The corresponding positions of melting point of coating and substrate can be observed, so the cross-section of cladding layer can be accurately determined.

As shown in Fig.3a, the temperature on the electron beam cladding layer is decreased with increasing the distance away from the beam spot center. The maximum temperature at distance of 2.5 mm is 1159 °C, whereas that of 3 mm is 722 °C. The melting point of the coating is 1100 °C. Thus, the half width of the cladding layer is about 2.5 mm[13]. Combined with Fig.3a and Fig.4a, it can be inferred that the melting width of the coating in the simulation model is approximately 5.1 mm. The peak temperature on the substrate surface is 2052 °C, the maximum temperature at depth of 1 mm of the substrate is 965 °C, and the melting point of the substrate is 1320 °C. Combined with Fig.3b and Fig.4b, the molten pool depth of the substrate is determined as 0.65 mm (coating thickness is 1 mm). The temperature at the interface between substrate and coating is also decreased with increasing the distance away from the beam spot center. The maximum temperature at depth of 1.5 and 2 mm of the substrate is 1548 and 961 °C, respectively. Combined with Fig. 3c and Fig. 4c, the molten pool width of the substrate can be determined as 3.4 mm. Through the simulation and analysis of molten pool width based on coating and substrate as well as the molten pool depth, the cross-section size of cladding layer under different processing parameters can be obtained, as listed in Table 1.

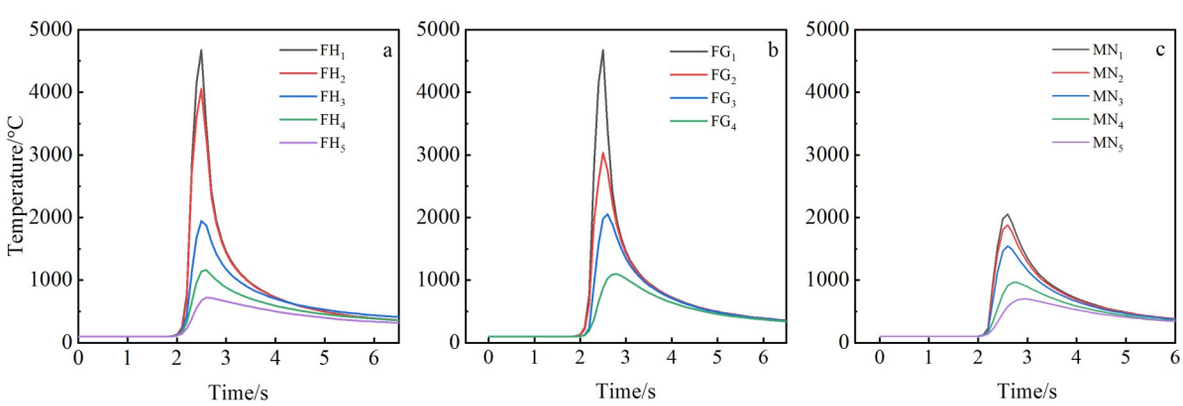

Fig.3 Temperature distributions of segmented lines on different typical paths of electron beam cladding: (a) FH lines, (b) FG lines, and (c) MN lines

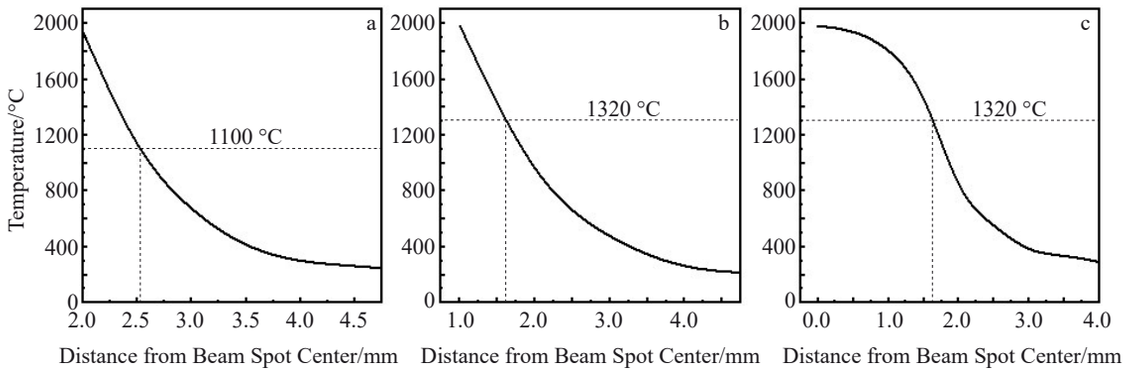

Fig.4 Maximum temperatures of electron beam cladding layer at different distances away from beam spot center along different typical paths: (a) FH line, (b) FG line, and (c) MN line

Table 1 Simulated cross-section sizes of cladding layer under different processing parameters

Specimen	Electron beam current/mA	Focus current/mA	Scanning speed/mm·s^{-1}	Substrate melting depth/mm	Coating melting width/mm	Substrate melting width/mm
1	17	680	6	0.11	5.60	1.50
2	17	690	8	0.30	5.24	3.36
3	17	700	10	0.65	5.10	3.40
4	20	680	8	0.09	5.72	1.96
5	20	690	10	0.27	5.36	3.50
6	20	700	6	1.26	6.02	4.20
7	23	680	10	0.09	5.74	2.08
8	23	690	6	1.03	6.22	4.60
9	23	700	8	1.28	5.94	4.06

2 Experiment

2.1 Methods and materials

The electron beam integrated processing system was used in this research. The performance parameters of the equipment were as follows: the acceleration voltage was 0–60 kV, the electron beam current was 0–120 mA, the scanning frequency was 0–600 Hz, and the focusing current was 0–1000 mA. The schematic diagram of electron beam cladding[14] equipment is shown in Fig.5.

Inconel 718 alloy is a nickel-based superalloy with precipitation reinforcement, which usually contains Ni, Fe, and Cr as the substrate and Nb and Mo additives. The microstructure of Inconel 718 alloy is mainly composed of austenite, and its chemical composition is shown in Table 2. Inconel 718 alloy has the advantages of high strength, strong oxidation resistance, and strong corrosion resistance[15]. However, under long-term service at high temperatures, the surface hardness of Inconel 718 alloy cannot meet the application requirements. As a nickel-based soluble alloy, NiCrBSi alloy has excellent wear resistance, excellent corrosion resistance, great oxidation resistance, and particularly high hardness due to the existence of chromium, boron, silicon, and other elements. The chemical composition of NiCrBSi powder is shown in Table 3[16]. The NiCrBSi coating was prepared on the surface of Inconel 718 alloy by electron beam cladding in order to improve the surface properties.

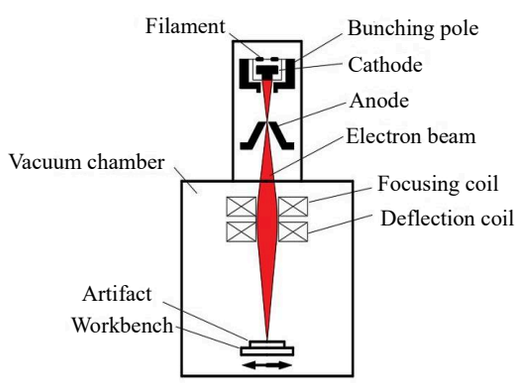

Fig.5 Schematic diagram of electron beam cladding equipment

Table 2 Chemical composition of Inconel 718 alloy (wt%)

Ni	Cr	Ti	Mo	Nb	Co	C	Mn	Si	S	Cu	Al	Fe
55	21	1.15	3.3	5.5	1	0.08	0.35	0.35	0.015	0.3	0.8	Bal.

Table 3 Chemical composition of NiCrBSi powder (wt%) [16]

Cr	B	Si	C	Fe	Ni
12	3.5	4.7	0.9	5.0	Bal.

2.2 Experimental cross-section size of cladding layer

The experimental cross-section size of the cladding layer after electron beam cladding was measured by metallographic method, and the results are shown in Table 4. The comparison between simulated and experimental cross-section sizes of cladding layer under different processing parameters is shown in Fig.6.

2.3 Calculation of dilution ratio of cladding layer

Scanning electron microscope (SEM) coupled with energy dispersive spectroscope (EDS) was used to conduct the composition analysis of the cross-section of cladding layer. In this research, three areas were selected at the cladding zone, substrate, and bonding zone, and the their composition was analyzed, as shown in Fig.7.

As shown in Fig. 7, the elements in the cladding zone and substrate all exist in the bonding zone, and the element content in the bonding zone is mostly higher than that in the substrate and cladding zone, which indicates that both the coating and the substrate are melted. It can also be seen that a small amount of Mo and Ti appears in the cladding zone, suggesting that in the process of electron beam cladding, the elements are transferred to the cladding zone, and the composition of cladding layer changes.

To calculate the dilution ratio of cladding layer, it is assumed that the substrate and coating are homogeneous and isotropic, and their physical parameters will not change due to mutual fusion. Additionally, neither the electron beam current, the broadening phenomenon of cladding layer, nor the variation of molten pool depth is considered during the calculation.

Table 4 Experimental cross-section sizes of cladding layer under different processing parameters

Specimen	Electron beam current/mA	Focus current/mA	Scanning speed/mm·s^{-1}	Substrate melting depth/mm	Coating melting width/mm	Substrate melting width/mm
1	17	680	6	0.16	5.02	1.94
2	17	690	8	0.24	4.76	2.64
3	17	700	10	0.52	4.70	2.58
4	20	680	8	0.14	5.26	1.66
5	20	690	10	0.20	5.02	2.72
6	20	700	6	0.80	5.50	3.84
7	23	680	10	0.12	5.10	1.74
8	23	690	6	0.74	5.36	3.82
9	23	700	8	0.82	5.24	4.10

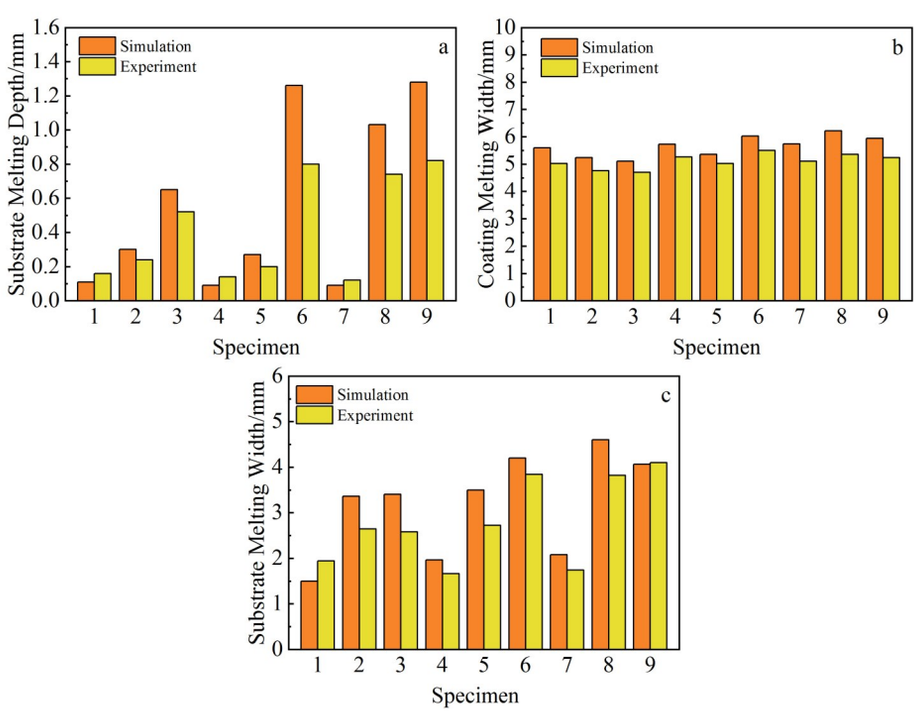

Fig.6 Comparison of simulated and experimental cross-section sizes of cladding layer under different processing parameters: (a) substrate melting depth, (b) coating melting width, and (c) substrate melting width

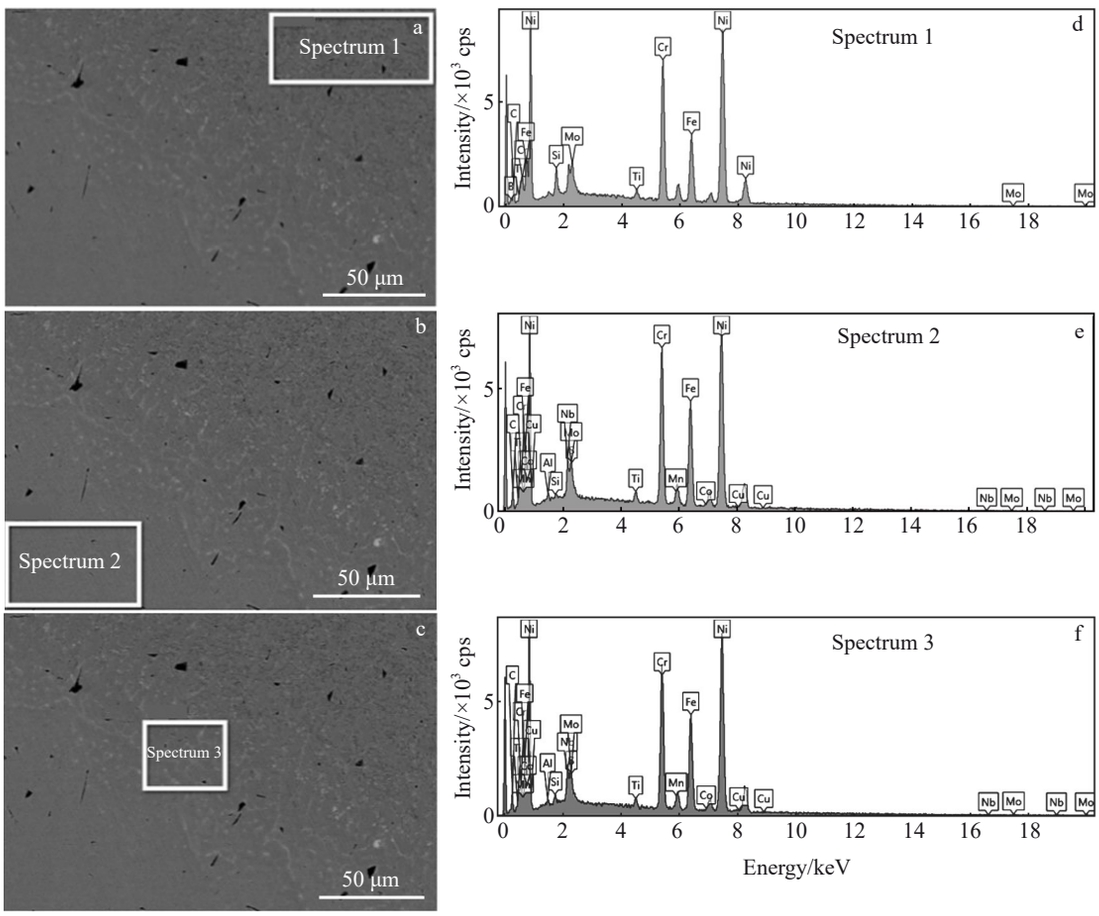

Fig.7 SEM morphologies (a–c) and EDS spectra (d–f) of cladding zone (a, d), substrate (b, e), and bonding zone (c, f) of NiCrBSi-coated Inconel718 alloy by electron beam cladding

The beam spot diameter of the electron beam was set as R and the scanning velocity of the electron beam was set as V_S. Thus, the action time t_0 can be expressed by Eq.(5), as follows:

$$t_0 = \frac{R}{V_s} \tag{5}$$

The mass of the coating and substrate during electron beam cladding can be calculated by Eq.(6) and Eq.(7), respectively, as follows:

$$M_r = \frac{2}{3} DH_r V_s \rho_r t_0 \tag{6}$$

$$M_j = \frac{2}{3} DH_j V_s \rho_j t_0 \tag{7}$$

where M_r is the melting mass of coating; M_j is the melting mass of substrate; ρ_j is the density of substrate material; ρ_r is the density of coating; D is the coating melting width; H_j is the substrate melting depth; H_r is the melting thickness of the coating layer (the coating thickness is 1 mm). Besides, d is the substrate melting width. Thus, based on the schematic diagram of the molten pool (Fig.8), the dilution ratio (η)[17] of electron beam cladding layer can be calculated, as follows:

$$\eta = \frac{M_j}{M_j + M_r} = \frac{H_j \rho_j}{H_j \rho_j + 0.75(D + d) H_r \rho_r} \tag{8}$$

The calculated dilution ratios at the center of the cladding layer are shown in Table 5. It can be seen that the simulated and experimental dilution ratios of cladding layer are quite similar to each other under the same conditions. Additionally,

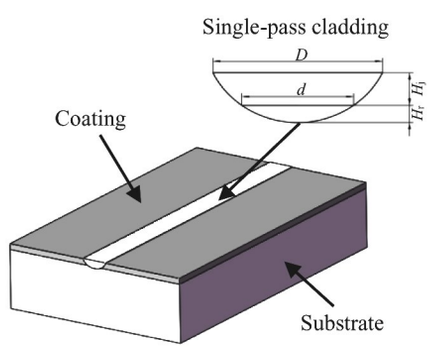

Fig.8 Schematic diagram of cross-section of molten pool during electron beam cladding

Table 5 Simulated and experimental dilution ratios (η) of cladding layers under different processing parameters (%)

Specimen	1	2	3	4	5	6	7	8	9
Simulated	3.28	14.6	27.5	3.24	13.47	43.04	3.37	38.98	43.12
Measured	6.11	11.10	21.19	4.67	9.30	32.43	4.26	31.00	28.26

the difference in dilution ratio of different experimental results is obviously smaller than that of different simulated results. The variation trends of dilution ratio of cladding layer and the substrate melting depth are basically the same. Obviously, the dilution ratio is positively correlated with the substrate melting depth. The cross-section shape of the cladding layer is semicircle. Under the same melting depth of cladding layer, the coating melting width and substrate melting width will not change significantly. When the melting depth of cladding layer changes, the melting volume and mass of the cladding layer change consequently, therefore changing the dilution ratio of cladding layer. The melting depth is greatly affected by the focus current value, so the dilution ratio is also affected by the focus current value.

3 Results and Discussion

3.1 Metallographic structure

In the process of electron beam cladding, the surface properties of cladding layer was also evaluated by observing the compactness of cladding layer structure and the defects, such as cracks and pores. Fig. 9 shows SEM morphologies of the cross-section of the cladding layer prepared by electron beam cladding. It can be seen from Fig. 9a that the cladding layer has three parts: (1) the cladding zone; (2) the bonding zone, i.e., the alloying zone (elongated white bright band)[18]; (3) Inconel 718 substrate. The area between the substrate and bonding zone is also called as the heat-affected zone, which is affected by the thermal energy of the electron beam in the process of electron beam cladding. Although the temperature at the heat-affected zone cannot reach the melting temperature, the structure of heat-affected zone is still transformed. Therefore, the characteristics of the heat-affected region are different from those of the cladding layer or those of the substrate.

It is clear that the cladding layer presents the dilution phenomenon, as shown in Fig. 9b. The coating along the melting path is completely melted and the substrate is partially melted. NiCrBSi coating has a good combination with Inconel 718 alloy, and there is a clear bonding line between the cladding layer and the substrate. The microstructure in the upper part of the cladding layer is coarse, and the quenching microstructure is distributed in the lower part of the cladding layer and in the heat-affected zone. Fig. 9c shows that after electron beam cladding, the defects, such as pores and cracks, in the cladding layer are obviously reduced, indicating that the electron beam cladding can reduce the defects in the substrate material.

3.2 Property analysis

In the hardness test, a series of points were selected to measure the Vickers hardness. The test loading mass was 200 g, and the loading time was 15 s.

Fig. 10 shows the Vickers hardness distribution of different cladding layers along the maximum penetration path. The hardness of the cladding zone is 6370 – 7350 MPa[19], that of the heat-affected zone gradually decreases, and the substrate hardness is about 4802 MPa[20]. As shown in Fig. 10, the cladding zone corresponds to the area with distance of 0 – 2 mm from the upper surface of cladding layer. The transition zone and the heat-affected zone correspond to the area with distance of 2 – 3.5 mm from the upper surface of cladding layer. The substrate locates at the area with distance greater than 3.5 mm from the cladding layer surface.

When the cladding temperature is too high, the surface alloying elements will be destroyed, thereby decreasing the hardness. Besides, when the heat source caused by laser beam leaves the cladding layer surface, the subsurface of the molten pool is in direct contact with the substrate. The substrate temperature is low, so the subsurface solidifies immediately. The surface of molten pool then releases heat to the surrounding area and also transfers heat to the substrate, thereby achieving solidification. In this case, the solidified subsurface of the molten pool will undergo microstructure transformation due to the reheating. Therefore, the characteristics of cladding layer is very uneven due to the rapid cooling and reheating. The quenching microstructure is distributed in the heat-affected zone of molten pool and subsurface. The temperature of the substrate adjacent to the heat-affected zone does not reach the transformation temperature, resulting in the tempering structure of the original substrate material. Therefore, the larger hardness appears in the subsurface of the molten pool.

It can also be seen from Fig. 10 that the smaller the dilution ratio, the higher the hardness of cladding layer and the more uniform the hardness distribution.

The substrate and the cladding layer with the smallest dilution ratio were used for friction tests. The test load was 20

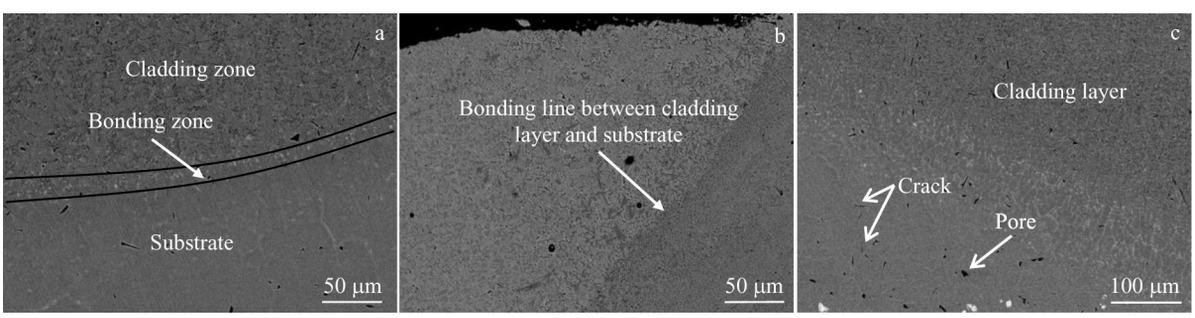

Fig.9 SEM morphologies of NiCrBSi coating on Inconel 718 alloy by electron beam cladding: (a) overall morphology; (b) bonding line between cladding layer and substrate; (c) surface defects

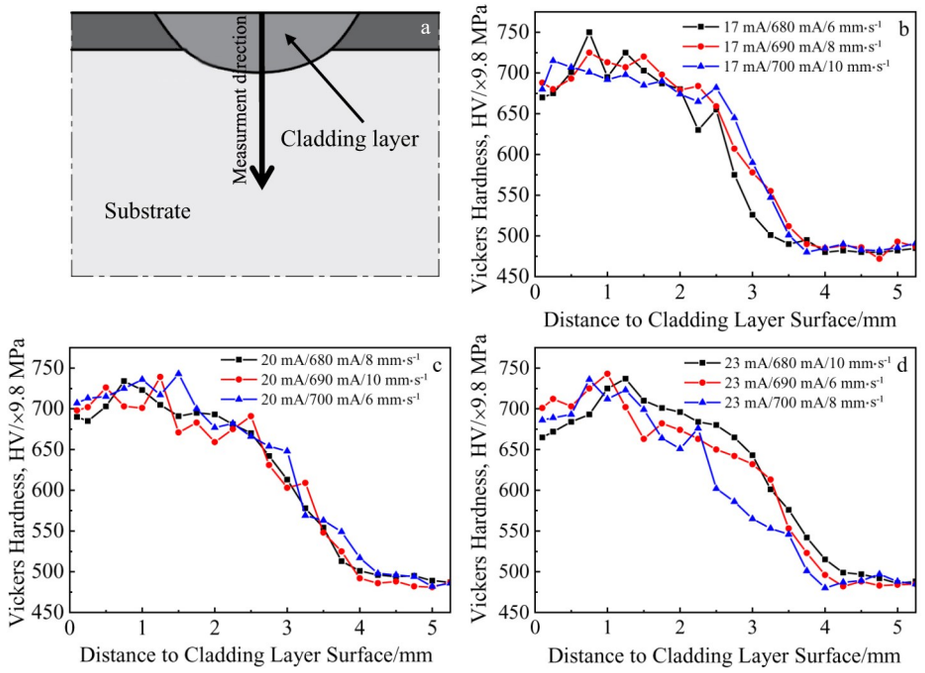

Fig.10 Schematic diagram of Vickers hardness measurement (a); Vickers hardness distributions of different cladding layers along the maximum penetration path: (b) specimens 1–3, (b) specimens 4–6, and (c) specimens 7–9

N, the loading time was 10 min, the reciprocating condition was 200 t/m, and the reciprocating length was 4 mm. With the constant friction speed, friction load, and grinding material, the small friction coefficient indicates the strong wear resistance of materials[21]. As shown in Fig. 11, the friction coefficient of Inconel 718 alloy substrate increases slowly firstly and then fluctuates around a constant value. This is because at the beginning of the friction experiment, it is at the running-in state. Afterwards, the experiment enters a stable state, and the average friction coefficient of the substrate during the whole friction process is 0.49. The friction coefficient of the cladding layer fluctuates greatly during the whole friction test, because the surface flatness of the cladding layer is low, and the protruding part of the surface is worn off at the beginning of friction experiment. The relative hardness of the cladding layer is high, and the worn-off part becomes

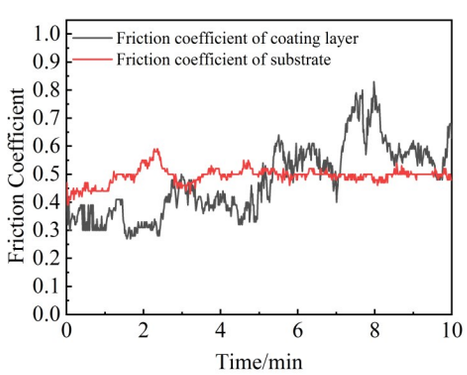

Fig.11 Friction coefficients of cladding layer and substrate during friction test

abrasive particles during the test. The welding-on phenomenon occurs on the contact surface due to the effect of pressure and molecular binding force. With the friction test proceeding, the contact surface is torn and the debris is produced, resulting in the large fluctuation in friction coefficient during the whole process. However, the average friction coefficient of the cladding layer is about 0.47, which is still lower than that of the substrate. This result indicates that the wear resistance of the cladding layer with small dilution ratio is better than that of the substrate. As a result, the quality of the cladding layer with a small dilution ratio is excellent.

4 Conclusions

1) The approximate melting range of the cladding layer can be obtained by analyzing the isotherm diagram of simulation model, the approximate cross-section size of the cladding layer can be determined, and then the simulated dilution ratio of cladding layer can be calculated. It is feasible to determine the cross-section size of the cladding layer by simulation.

2) The simulated and experimental results of the dilution ratio have basically the same variation trends under different processing parameters. However, the simulated and experimental substrate melting depths have a relatively large deviation. The simulated and experimental coating/substrate melting widths are similar to each other, and their variation trend is similar to that of the dilution ratio, indicating that the dilution ratio is mainly affected by the melting depth. The melting depth is greatly affected by the focus current value, so the dilution ratio is also affected by the focus current value.

3) The cladding layer with a small dilution ratio has uniform microstructure and high hardness. The wear resistance of cladding layer with a small dilution ratio is also

better than that with high dilution ratio. It can be seen that after electron beam cladding, the wear resistance of the cladding layer is improved.

References

1 Zhang Guopei, Liu Hailang, Huang Yiping *et al*. *Hot Working Technology*[J], 2017, 46(2): 27 (in Chinese)

2 Liu Hailang, Wang Bo, Qi Zhengwei *et al*. *Rare Metal Materials and Engineering*[J], 2018, 47(11): 3338 (in Chinese)

3 Xi W C, Song B X, Zhao Y *et al*. *The International Journal of Advanced Manufacturing Technology*[J], 2019, 103: 4695

4 Mohammed S, Zhang Z, Kovacevic R. *The International Journal of Advanced Manufacturing Technology*[J], 2020, 111: 2553

5 Zhang Qingmao, Zhong Minlin, Yang Sen *et al*. *Heat Treatment of Metals*[J], 2001, 26(8): 20 (in Chinese)

6 Huang Yongjun, Zeng Xiaoyan, Hu Qianwu *et al*. *Journal of Applied Optics*[J], 2008, 29(2): 248 (in Chinese)

7 Utu D, Brandl W, Marginean G *et al*. *Vacuum*[J], 2005, 77: 451

8 Tian H C, Chen X D, Yan Z H *et al*. *Applied Physics A*[J], 2019, 125(7): 485

9 Xu Ruihua. *Research of Preparation and Simulation of Ti-Al Laser Cladded Coating Reinforced by Nano Powder on Aluminum Alloy*[D]. Nanjing: Nanjing University of Aeronautics and Astronautics, 2014 (in Chinese)

10 Wu Yanpin, Zhang Jing. *Foundry Technology*[J], 2014, 35(12): 2903 (in Chinese)

11 Wu Ping. *Numerical Simulation of Laser Welding and Brazing of Aluminum Alloy-Galvanized Steel and Optimization of Process Parameters*[D]. Changsha: Hunan University, 2012 (in Chinese)

12 Lu Jinbin, Meng Pu, Peng Zhuqin *et al*. *Journal of Zhongyuan University of Technology*[J], 2009, 20(5): 10 (in Chinese)

13 Li Jianzhong. *Preparation and Simulation Research of Al/Ti Laser Cladding Coating on 7050 Aluminum Alloy*[D]. Nanjing: Nanjing University of Aeronautics and Astronautics, 2015 (in Chinese)

14 Yu Haihua. *Study on the Surface Remelting of Cu-Cr Alloy Contact with High Energy Electron Beam*[D]. Guilin: Guilin University of Electronic Technology, 2015 (in Chinese)

15 Yao Dengzhi. *Numerical Simulation Research on Laser Cladding Inconel718 Alloy*[D]. Lanzhou: Lanzhou University of Technology, 2019 (in Chinese)

16 Fen Jing, Zhang Bing, Jiang Qiutong *et al*. *China Southern Agricultural Machinery*[J], 2020, 51(5): 37 (in Chinese)

17 Zhong Song. *Simulation and Experimental Research on Temperature Field of Cr12MoV Die Steel Electron Beam Cladding*[D]. Guilin: Guilin University of Electronic Technology, 2014 (in Chinese)

18 Jiao Shaobin. *Study on Preparation Process and Wear Resistance of SiC Coating Cladding on Die Steel Surface*[D]. Xiangtan: Xiangtan University, 2012 (in Chinese)

19 Zhao Kaihua, Sun Ronglu, Niu Wei *et al*. *Optical Technique*[J], 2009, 35(2): 232 (in Chinese)

20 Feng Jun, Jin Fanya, Tong Honghui *et al*. *Hot Working Technology*[J], 2015, 44(4): 184 (in Chinese)

21 Li Yan. *Laser Cladding Composite Coating of Aluminum Bronze Matrix on Magnesium Alloy Surface*[D]. Taiyuan: Taiyuan University of Technology, 2011 (in Chinese)

Inconel 718合金电子束熔覆稀释率的数值仿真与实验

徐珑韬[1]，杨　伟[1]，刘海浪[2]，彭治国[2]，刘　建[1]

(1. 中国电子科技集团公司 第三十研究所，四川 成都 611730)

(2. 桂林电子科技大学 机电工程学院，广西 桂林 541004)

摘　要：基于Ansys软件仿真电子束熔覆过程中的温度场分布规律，估测熔覆层截面熔化深度、熔化宽度值，进而通过仿真估测熔覆层稀释率值的大小，随后进行电子束熔覆实验并计算稀释率的实际值，对比模拟值与实际值的情况，确认通过仿真可得出电子束熔覆的稀释率值。测试熔覆后试样的显微硬度和典型试样的耐磨性能，结果表明稀释率值小的试样，熔覆层的质量更优异。

关键词：Inconel 718合金；电子束熔覆；温度场仿真；稀释率

作者简介：徐珑韬，男，1994年生，硕士，工程师，中国电子科技集团公司第三十研究所，四川 成都 611730，E-mail：2101486502@qq.com